Surface organization of aqueous $MgCl_2$ and application to atmospheric marine aerosol chemistry

Nadia N. Casillas-Ituarte[a], Karen M. Callahan[b], Cheng Y. Tang[a], Xiangke Chen[a], Martina Roeselová[c], Douglas J. Tobias[b], and Heather C. Allen[a,1]

[a]Department of Chemistry, The Ohio State University, 100 West 18th Avenue, Columbus, OH 43210, [b]Environmental Molecular Science Institute and Department of Chemistry, University of California, Irvine, CA 92697, and [c]Center for Biomolecules and Complex Molecular Systems, Institute of Organic Chemistry and Biochemistry, Academy of Sciences of the Czech Republic, Flemingovo nam. 2, 16610 Prague 6, Czech Republic

Edited by Barbara J. Finlayson-Pitts, University of California, Irvine, Irvine, CA, and approved January 11, 2010 (received for review November 2, 2009)

Inorganic salts in marine aerosols play an active role in atmospheric chemistry, particularly in coastal urban regions. The study of the interactions of these ions with water molecules at the aqueous surface helps to elucidate the role of inorganic cations and anions in atmospheric processes. We present surface vibrational sum frequency generation (SFG) spectroscopic and molecular dynamics (MD) studies of aqueous $MgCl_2$ surfaces as models of marine aerosol. Spectroscopy results reveal that the disturbance of the hydrogen bonding environment of the air/aqueous interface is dependent on the $MgCl_2$ concentration. At low concentrations (<1 M) minor changes are observed. At concentrations above 1 M the hydrogen bonding environment is highly perturbed. The 2.1 M intermediate concentration solution shows the largest SFG response relative to the other solutions including concentrations as high as 4.7 M. The enhancement of SFG signal observed for the 2.1 M solution is attributed to a larger SFG-active interfacial region and more strongly oriented water molecules relative to other concentrations. MD simulations reveal concentration dependent compression of stratified layers of ions and water orientation differences at higher concentrations. SFG and MD studies of the dangling OH of the surface water reveal that the topmost water layer is affected structurally at high concentrations (>3.1 M). Finally, the $MgCl_2$ concentration effect on a fatty acid coated aqueous surface was investigated and SFG spectra reveal that deprotonation of the carboxylic acid of atmospherically relevant palmitic acid (PA) is accompanied by binding of the Mg^{2+} to the PA headgroup.

magnesium chloride | fatty acid | air/aqueous interface | sum frequency spectroscopy | molecular dynamics

Inorganic salts present in marine boundary layer (MBL) aerosol originate from turbulent wave action at the surface of the ocean (1). These aerosols, typically of the micron size range and smaller, travel over continental regions by being entrained in the air mass in which they were created, and have been detected more than 900 km inland (2). Aerosols play a key role in the modification of global climate through their effect on cloud condensation nuclei prevalence, radiative balance, and level of precipitation (3). Aerosol composition and size have also been correlated to thunderstorm severity (4). Alkali metals (Na, K, Li, and Rb), alkaline earth metals (Mg, Ca), and ammonium (NH_4^+) make up the majority of cationic species, and halides (F, Cl, Br, and I) and oxidized sulfur and nitrogen ions make up the majority of inorganic anionic species found in MBL aerosol (5, 6). While calcium and magnesium are the most prevalent divalent cations in seawater and MBL aerosols, chloride anion is the dominant halide species (5). Although recent cloud drop measurements in the MBL show that calcium concentrations are about four times higher than magnesium concentrations, (6) the small size and high charge density of Mg^{2+} gives rise to a strongly hydrated complex in aqueous solution, contributing to its limited ability to form contact ion pairs with anions such as nitrate and chloride (7). This trait may also result in an unusual impact on surface and subsurface physical properties of MBL aerosol.

Within the MBL, halide chemistry is of global importance because of its crucial role in ozone creation and alternatively, ozone depletion events (8). For example, chlorine radical reacts faster with hydrocarbons than hydroxyl radical. When chlorine radical and NO_x concentrations reach threshold values, ozone production is dominated by chlorine radical chemistry (9). This has a major impact on air quality in many coastal urban regions of the world. Recent modeling studies suggest that the formation and self-reaction of surface $OH\cdots Cl^-$ complexes is an important route to molecular chlorine which then photochemically produces two chlorine radicals, and that large and polarizable halide anions like chloride play a significant role at the surfaces of aqueous particles (8).

There are many unanswered questions concerning MBL aerosols. How do environmentally available ions and surface-active organic molecules organize at the surface of MBL aerosols? How do counter cations and organic molecules affect the chemistry of MBL aerosols, for example chloride availability and reactivity? While most environmentally available cations readily ion pair to chloride, the unique size and high charge density of Mg^{2+} allow it to remain hydrated by six waters, so that it does not form a contact ion pair with Cl^- even at high concentrations (7). Could this unusual behavior perturb the surface and subsurface of atmospheric aerosols and play a role in chloride activity and availability? Given the strong ability of magnesium to hold onto water, how does concentration affect the interfacial region of aqueous solutions with magnesium? Additionally, MBL aerosol compositions are complex and can contain hundreds of organic species (10). Of the organics, short chain dicarboxylic (6) and long chain fatty acids such as palmitic acid (11), as studied here, sometimes dominate the organic fraction.

The study of the interactions between inorganic salts and water molecules that occur during ion solvation is fundamental to understanding the role of ions in biological, geological, and environmental processes, in particular, in atmospheric aerosol processes. In this paper we address these fundamental interactions and resulting surface perturbations to surface aqueous structure, and we explore the complexity that arises from biologically derived fatty acid coatings on aqueous surface phenomena. We present vibrational sum frequency generation (SFG) spectroscopic studies of aqueous surfaces relevant to

Author contributions: N.N.C.-I., K.M.C., C.Y.T., and X.C. performed research; N.N.C.-I., K.M.C., C.Y.T., X.C., M.R., D.J.T., and H.C.A. analyzed data; N.N.C.-I., K.M.C., D.J.T., and H.C.A. wrote the paper; D.J.T. and H.C.A. designed research.

The authors declare no conflict of interest.

This article is a PNAS Direct Submission.

[1]To whom correspondence should be addressed. E-mail: allen@chemistry.ohio-state.edu.

This article contains supporting information online at www.pnas.org/cgi/content/full/0912322107/DCSupplemental.

www.pnas.org/cgi/doi/10.1073/pnas.0912322107

understanding the perturbation caused by marine aerosol concentrations of $MgCl_2$. The SFG results are complemented with molecular dynamics (MD) simulations that provide an atomistic view of the surfaces of aqueous $MgCl_2$.

Results

Vibrational Spectroscopy of the Air/Aqueous Interface. We report surface water organization and structure from interpretation of aqueous $MgCl_2$ SFG spectra. SFG spectra under the ssp polarization combination (s polarized SFG, s polarized incident visible, p polarized infrared) of 0.1 M, 0.3 M, 1.1 M, 2.1 M, 3.1 M, and 4.7 M aqueous $MgCl_2$ are shown in Fig. 1*A* and *B*. Before $MgCl_2$ addition, the spectrum of neat water reveals a broad continuum that spans from 3,000 to 3,600 cm^{-1} and is assigned to the OH stretching modes of hydrogen-bonded water molecules. The assignments within this continuum are controversial and still under discussion (12); however, as the frequency of the OH stretching modes increases, the strength of the hydrogen bonds between water molecules decreases (12, 13). This spectral region is also affected by coupling (14) and the collective nature of the vibrations (13). At 3,700 cm^{-1} a narrow peak is observed and is assigned to the free OH of water molecules that straddle the air/aqueous interface with one OH bond uncoupled and oriented toward the gas phase and the other OH interacting through hydrogen bonding with the water molecules in the liquid phase (15).

$MgCl_2$ concentrations less than 1.0 M are shown in Fig. 1*A*. These SFG spectra reveal only minor changes relative to water. For the 0.1 M and 0.3 M aqueous solutions, a slight spectral narrowing is observed at the edges of the hydrogen bonding region at 3,000 and 3,600 cm^{-1}. In the 0.3 M solution spectrum, a small intensity enhancement is observed around 3,300 cm^{-1}. The free OH region at 3,700 cm^{-1} shows no change relative to water.

For $MgCl_2$ concentrations of 1.1 M, 2.1 M, 3.1 M, and 4.7 M, the SFG spectra in Fig. 1*B* show a significant intensity enhancement around 3,300 cm^{-1} accompanied by an increase in the narrowing of the low and high frequency edges of the hydrogen bonding region as one increases the $MgCl_2$ concentration *. By analyzing the spectra of Fig. 1*A* and *B* using parameters identified through phase analysis of aqueous salt solutions by Shen and coworkers (16), one band at ~3,200 cm^{-1} with positive phase and a second band at ~3,400 cm^{-1} with negative phase fit the spectra rather well (Table S1). Additionally, peaks at ~3,650, 3,700, and 3,750 cm^{-1} were used, all with positive phase. We have also tested the band amplitudes by increasing the nonresonant term (Eq. **2**) (17). Through the analysis, we observe that the apparent narrowing of the hydrogen bonding region can also be interpreted as a blue shift of the ~3,200 band and a red shift of the ~3,400 band with increasing salt concentrations. Although spectral narrowing may be associated with an increase in lifetime of the hydrogen bonds in the hydrogen bonding network, it is difficult to ascertain here.

The spectral intensity at ~3,300 cm^{-1} increases in the order of 0.1 M, 0.3 M, 1.1 M, and 2.1 M, and then decreases with concentration above 2.1 M; the 4.7 M spectrum nearly overlaps with the 1.1 M spectrum in the hydrogen bonding region. Noncentrosymmetric hydrogen bonding structures may extend deeper below the surface of the 2.1 M solution relative to the other solutions studied here. Application of the SFG selection rule, lack of inversion symmetry requirement for SFG activity, provides indirect data on concentration gradients in the interfacial region up until the SFG coherence length upon reflection. However, an increase in the ordering of the water dipole will also increase the intensity since SFG is highly sensitive to orientation.

Contrary to the maximum 3,300 cm^{-1} intensity observed in the hydrogen bonding region for the 2.1 M solution in Fig. 1*B*, the intensity of the free OH peak centered at 3,700 cm^{-1} for neat water is reduced in accordance with decreasing water content (increasing salt concentration), as expected, although the intensity reduction is rather modest. The 3,700 cm^{-1} peak is discussed later with respect to polarization analysis of SFG spectra and MD simulation results.

A small broad peak at 3,650 cm^{-1} in the SFG spectra of Fig. 1*B* is observed and becomes more easily discernable because of the narrowing of the hydrogen bonding region at higher concentrations. We have confirmed through a temperature study that this peak is due to a free OH bond and not involved in hydrogen bonding (*SI Appendix*). A free OH of interfacial water molecules with their oxygens interacting with Mg^{2+} or with the Mg^{2+} solvation shell likely contributes to this band (18). A peak in this spectral region was also observed by others and assigned to the symmetric stretch of the decoupled free OH and donor-bonded OH of three-coordinate water molecules (16) and weakly hydrogen-bonded water molecules (19).

Comparison of the data in Figs. 1*A* and *B* to previously published surface water structure spectra of other salts reveals some interesting differences. SFG spectra of aqueous sodium halide (12, 13), ammonium and sodium sulfate (13), and divalent-cation nitrate salt solutions (12) reveal enhancements in the 3,400 cm^{-1} region, although the aqueous ammonium chloride salt spectrum (13) showed enhancement at 3,300 cm^{-1} as is observed here for $MgCl_2$. Also different than observed in Fig. 1, a significant loss in intensity in the 3,200 cm^{-1} region was observed in SFG spectra of aqueous alkaline earth (Mg^{2+}, Ca^{2+}, and Sr^{2+}) nitrate solutions, and a relatively unperturbed 3,400 cm^{-1} band frequency was observed in SFG spectra of aqueous $Mg(NO_3)_2$ (12).

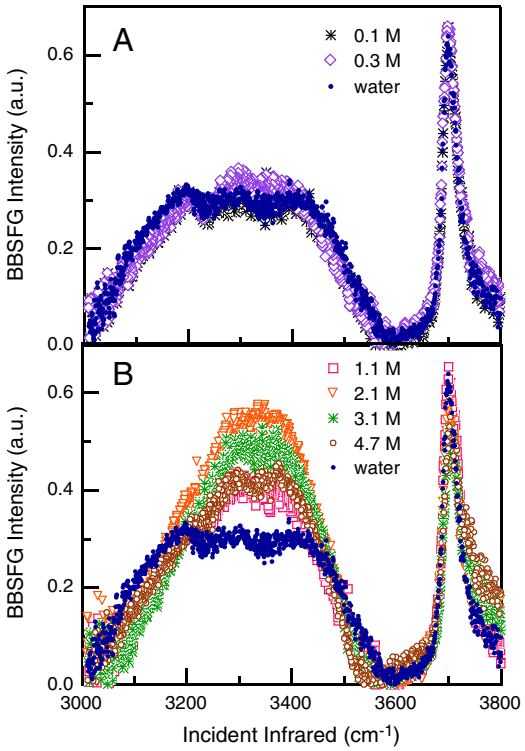

Fig. 1. SFG spectra of aqueous $MgCl_2$ solutions of A) 0.1 M and 0.3 M and B) 1.1 M, 2.1 M, 3.1 M, and 4.7 M. Neat water spectrum is also shown for reference.

*Previously, we reported SFG intensity that was slightly reduced relative to water for a 1 M $MgCl_2$ solution (ref. 12), although the shape of the spectrum reported here is nearly identical. The reduced intensity of the 1 M aqueous $MgCl_2$ spectrum as published in ref. 12 was due to an artifact caused by faulty alignment of the scanning system SFG detection optics that has since been corrected.

Vibrational Spectroscopy of the Bulk Solution and Spectral Analysis. In this study, we have acquired Raman and infrared vibrational spectra from the same bulk solutions (Figs. S2 and S3 in *SI Appendix*) as were used in the SFG studies. SFG spectral component peaks can be related to the parallel-polarized Raman and IR component peaks because of the mathematical relationship between SFG intensity and Raman multiplied by the IR transition moments as shown in Eq. (**1**).

$$I_{\mathrm{SFG}} \propto \beta_{lmn,\nu} \propto \langle g|\alpha_{lm}|\nu\rangle\langle\nu|\mu_n|g\rangle \qquad [1]$$

I_{SFG} is the SFG intensity, $\beta_{lmn,\nu}$ is the second-order hyperpolarizability, $\langle g|\alpha_{lm}|\nu\rangle$ represents the Raman tensor for the transition, $\langle\nu|\mu_n|g\rangle$ describes the IR transition moment, and *lmn* defines the molecule-fixed axes.

Coherence effects, and therefore interference, of the SFG photons as shown in Eq. (**2**) are taken into account for comparison to the simple additivity of Raman and infrared component peaks.

$$I_{\mathrm{SFG}} \propto |\chi^{(2)}|^2 \propto \left|\chi^{(2)}_{\mathrm{NR}} + \sum_{\nu}\chi^{(2)}_{\nu}\right|^2 \qquad [2A]$$

$$\chi^{(2)}_{\nu} \propto \frac{A_{\nu}}{\omega_{\nu} - \omega_{\mathrm{IR}} - i\Gamma_{\nu}} \qquad [2B]$$

In Eq. (**2A**), $\chi^{(2)}$ is the second-order nonlinear susceptibility, $\chi^{(2)}_{\mathrm{NR}}$ is the nonresonant term, and $\sum\chi^{(2)}_{\nu}$ is the summation of the resonant terms. Eq. (**2B**) reveals the Lorentzian lineshape of the resonant macroscopic susceptibility. In Eq. (**2B**), A_{ν} is the amplitude of the SFG transition moment, ω_{ν} is the frequency of the transition, and Γ_{ν} describes the line width of the transition.

In accordance with Eq. (**1**), we have analyzed in Fig. S4 in *SI Appendix* the parallel-polarized Raman and transmission IR spectra acquired from the bulk solutions to compare to the ssp polarized SFG spectra from the air/aqueous interfaces for intensity and frequency trends. The analysis suggests that the response of the hydrogen bonding environment to increasing salt concentrations is different at the surface compared to the bulk, and that the 2.1 M $MgCl_2$ solution is unique.

Free OH Region of the SFG Spectra. The free OH stretch at $3,700\ \mathrm{cm}^{-1}$ was investigated in a separate set of SFG experiments to elucidate intensity and frequency changes of the aqueous $MgCl_2$ surfaces relative to neat water. In Fig. 2, ssp polarized SFG spectra are shown (ppp polarized in Fig. S5 in *SI Appendix*). A $5\ \mathrm{cm}^{-1}$ blue shift of the free OH is observed from the lowest to the highest $MgCl_2$ concentration: However, the $3,700\ \mathrm{cm}^{-1}$ component peak of the spectral fits is observed to red shift with an increase in the magnitude of the nonresonant term. Therefore, due to the complexity of these spectra, we refrain from assigning the observed shift to a specific interfacial structure.

Upon further inspection of Fig. 2, a signal reduction with $MgCl_2$ concentration is revealed. This reduction is also observed after sensitivity testing of the nonresonant term in the fitting procedure (Table S1). Orientation analysis reveals that the ssp to the ppp intensity ratios do not change except in the case of the 3.1 M and 4.7 M solutions. For these higher concentrations the average orientation of the free OH is determined to be $31 \pm 2°$, whereas the free OH from neat water is determined to be $33 \pm 2°$ (Fig. S5 in *SI Appendix*). The angles are within the error of the orientation calculation where the main contributor is the spectral fits. Therefore, we assign the intensity reduction to a reduced number of free OH oscillators assuming that the free OH bandshape is not strongly affected by a change in the vibrational lifetime. The number density reduction of free OH of <10% based on the SFG spectra is smaller than one might expect by subtracting surface waters displaced by surface Cl^-.

Composition of the Interfaces by MD Simulations. MD simulations of the interfacial region of $MgCl_2$ solutions were carried out to develop a microscopic picture of the solution surfaces. The interfacial compositions are depicted by the density profiles shown in Fig. 3 (snapshots of the surface are shown in Fig. S6 in *SI Appendix*). The Gibbs dividing surface (GDS), which is approximated by the point along the Z-axis halfway between where the water density is 10% and 90% of the bulk water density, is set to $Z = 0$ Å, providing a common point of reference for each system. The density profiles reveal that Cl^- is present at the surface of all of the solutions, and the position of the surface Cl^- peak moves higher in the interface with increasing concentration. Right below the surface Cl^- peak, there is a considerable Mg^{2+} enhancement. In 1.1 M $MgCl_2$, it occurs at about 5 Å below the GDS, and also moves closer to the air/aqueous interface with increasing concentration. At 4.8 M there are very few water molecules that are not coordinating Mg^{2+}, and the solution resembles a disordered solid, manifested in the jaggedness of the density profiles. Additionally, we observe a second layer of enhanced

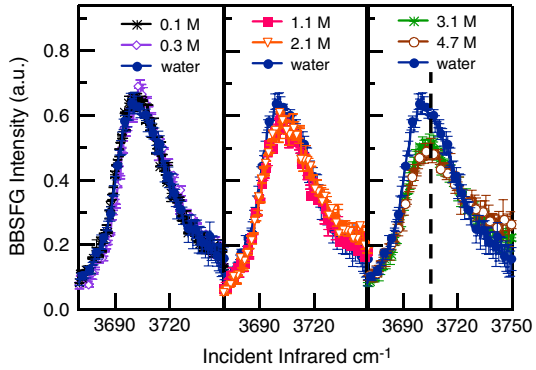

Fig. 2. SFG spectra in the free OH region of aqueous $MgCl_2$ solutions of 0.1 M, 0.3 M, 1.1 M, 2.1 M, 3.1 M, and 4.7 M using the ssp polarization combination. Neat water spectrum is also shown for reference.

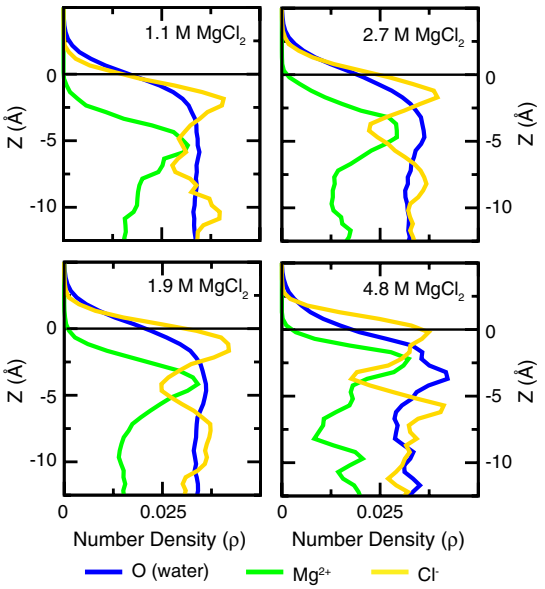

Fig. 3. Density profiles of water O atoms and Mg^{2+} and Cl^- ions. The density profiles are normalized so that the area under the curves for water and chloride is the same, i.e., $\int_{z\,\mathrm{min}}^{z\,\mathrm{max}}\rho(Z)dZ = 1$, and the areas for Mg^{2+} are 0.5 (i.e., the ratio of the numbers of Mg^{2+} and Cl^-).

Cl^- below the Mg^{2+} enhancement at all concentrations, which follows the trend of moving towards the interface as the $MgCl_2$ concentration increases.

MD Analysis of Free OH. To make contact with the SFG spectra, the orientational distribution of free OH bonds is presented in Fig. 4. Averaged net orientation order parameters and number density profiles of free OH bonds are presented in Fig. S8 in *SI Appendix*. A free OH bond is defined here as a water OH that is not a proton donor in a hydrogen bond to another water molecule or Cl^-, where hydrogen bonds are determined by distance and angle criteria. It is evident in Fig. 4 that free OH bonds with H atoms pointing into the vapor phase are enhanced near the interface in all of the systems. Below the GDS, increasing salt concentration results in an increasingly complicated distribution. In 1.1 M $MgCl_2$ the distribution is fairly similar to that of neat water, but with more free OH. In 1.9 M $MgCl_2$, deeper ordering of free OH is evident, and in 2.7 M and 4.8 M $MgCl_2$ layers of free OH with opposite orientation are apparent. Though the number of free OH observed by MD simulations increases with concentration, in the SFG spectra the signal from free OH decreases slightly with concentration. These differences are discussed in the *Discussion* Section.

$MgCl_2$ Aqueous Solutions and Palmitic Acid Monolayers. Palmitic acid (PA, $C_{15}H_{31}COOH$) spontaneously forms a monolayer on water and aqueous salt solutions with its carboxylic acid headgroup hydrated by the aqueous solution, and with its single hydrophobic tail (C_{15}) pointing into the air. Here, we investigate the effects that the fatty acid molecules have on the organization of the solvated Mg^{2+} and Cl^- ions. To evaluate the organization of the ions, we used deuterated PA ($C_{15}D_{31}COOH$) as a constituent of our model MBL solution. The headgroup structure, and thereby the interactions of the headgroup with the aqueous-phase ions, is elucidated.

In Fig. 5, SFG ssp polarized spectra of the acid headgroup of PA, i.e., the C = O stretch of the protonated PA at $\sim 1,700$ cm^{-1}, and the CO_2^- symmetric stretching (ss) modes of the deprotonated PA at $\sim 1,450$ cm^{-1} are shown. In the inset, the C = O stretch of the protonated acid from the same experiments is

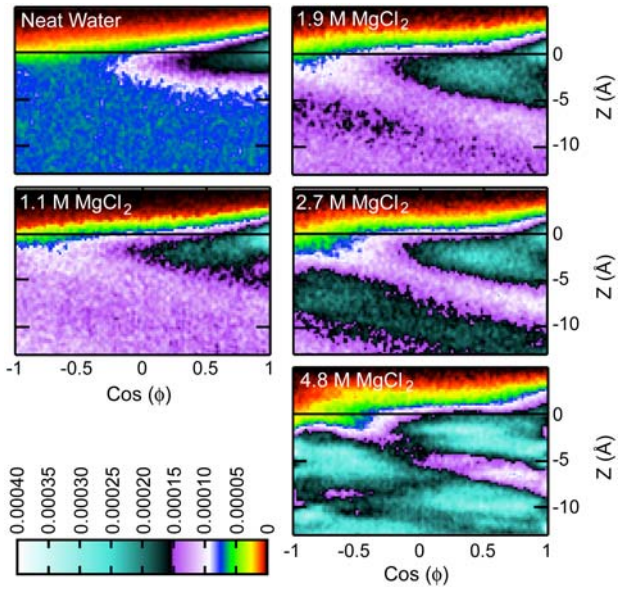

Fig. 4. Histograms of the density of free OH as a function of Z and $\text{Cos}(\phi)$, where ϕ is the angle between the OH vector and the Z-axis. The Gibbs dividing surface is at $Z = 0$. A positive value of $\text{Cos}(\phi)$ means that the H atom of the free OH points towards the vapor phase, above the slab.

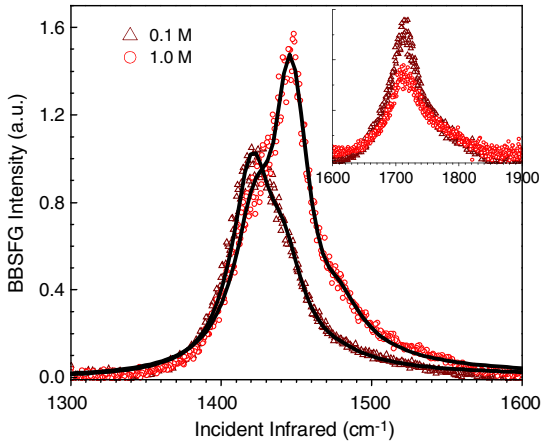

Fig. 5. SFG ssp spectra of the CO_2^- modes of deuterated (D31) palmitic acid with 0.1 M and 1.0 M $MgCl_2$ subphases. From the same experiments, spectra of the C = O region at ~ 1720 cm^{-1} shown in the inset.

observed to decrease with increasing $MgCl_2$ concentration, revealing a decrease in the number of protonated acid groups at the interface. In the main plot, the CO_2^- ss spectra reveal an increase in the associated spectral region of 1,400 to $1,480$ cm^{-1} with increasing $MgCl_2$ concentration, consistent with an increase in deprotonation of the PA headgroups. Both spectra contain component peaks at $1,424$ cm^{-1}, $1,445$ cm^{-1}, and $1,475$ cm^{-1} (spectral fits in Fig. S9 in *SI Appendix*). The lowest frequency peak found in the 0.1 M spectrum and as a shoulder in the 1.0 M spectrum is assigned to the hydrated CO_2^- headgroup of PA. The two higher frequency modes are assigned to a bound $Mg^{2+}:CO_2^-$ complex. These assignments are consistent with our previous studies on aqueous KCl (20). The mid frequency peak is dominant in the 1.0 M spectrum. As the concentration is increased from 0.1 M to 1.0 M $MgCl_2$, the low frequency mode is diminished while the mid and higher frequency modes are enhanced, revealing an increase in the number of Mg^{2+} that are coordinating the deprotonated PA headgroup.

With a fatty acid surface coating on an aqueous $MgCl_2$ solution, we also observe surface activity of the ions, but in this case it is the binding event that indicates that Mg^{2+} resides in the interfacial region. Surface activity of the Mg^{2+} is commensurate with deprotonation of the PA headgroups in the monolayer, followed by the binding of the Mg^{2+} to the deprotonated PA. The structural picture is different from that of the purely aqueous salt surface. Cl^- surface activity is promoting the surface activity of Mg^{2+} and therefore its surface approach to coordinate with the PA headgroup. The resulting binding event stabilizes Mg^{2+} in the subsurface region.

Discussion

Influence of Ions on the Bandshape and Intensity of the Hydrogen-Bonded Region of the Vibrational Spectra. In the bulk phase Raman and IR spectra (Figs. S2 and S3 in *SI Appendix*) there is an overall increase in intensity of the $3,400$ cm^{-1} peak with the addition of $MgCl_2$, while in the Raman the $3,200$ cm^{-1} peak is greatly diminished with increasing concentration. This is most noticeable at 4.7 M. Radial distribution functions of water around magnesium (*SI Appendix*) show increasing order beyond the second solvation shell of Mg^{2+} as the $MgCl_2$ concentration increases, both in the bulk and at the interface. As the concentration increases, a larger fraction of the water molecules are directly interacting with ions. Ab initio calculations on ion-water clusters suggested that an OH oscillator donating to Cl^- experiences a large increase in intensity (21). This has been observed for aqueous halide solutions from Raman spectra (22). These previous studies strongly suggest that

the increase in intensity of the IR and Raman spectra are at least in part due to increasing interactions of water molecules with ions.

Unlike the bulk hydrogen bonding region where the spectral intensity increases with $MgCl_2$ concentration, the spectral intensity of the air/aqueous solution interface does not follow a linear concentration trend. At low concentrations, increasing salt concentrations do increase the SFG spectral intensity in the hydrogen bonding region as with other salts, in agreement with the idea that addition of salt increases the width of the SFG-active interfacial layer. However, from the MD density profiles in Fig. 3, we also observe vertical compression of the stratified layers of salt enhancements with increasing concentration. At low concentrations this could cause the water to orient more strongly with increasing concentration. However, as higher concentrations are reached, this compression reduces the width of the noncentrosymmetric SFG-active environment, eventually causing the spectral intensity to start decreasing with increasing concentration (~2.1 M). The effect is considerable at 4.7 M.

Spectral Narrowing of the Hydrogen Bonding Region. Spectral narrowing in both the Raman and SFG spectra has been observed at every concentration of $MgCl_2$ considered here, and previously in NaCl solutions (12). The spectral narrowing, which has also been viewed as a red-shifting of the $3,400\ cm^{-1}$ peak and a blue shifting of the $3,200\ cm^{-1}$ peak in both Raman and SFG spectra, suggests a change in the hydrogen bonding network. The water-water interaction energy distributions presented in Fig. S7 in *SI Appendix* show that the addition of salt ($MgCl_2$ or NaCl) result in a loss of water-water hydrogen bonds (corresponding to the peak in the distributions between −2 and −5 kcal/mol). In aqueous NaCl there is a shoulder on the right side of the main peak in the distributions around 0 kcal/mol, which indicates that interactions with ions leads to unfavorable water-water interactions. In the $MgCl_2$ solutions there is a well-defined peak at positive interaction energies whose size increases with concentration. While addition of either salt is expected to disrupt water-water hydrogen bonds, it is clear that Mg^{2+} has a much greater disruptive influence on water-water hydrogen bonds than Na^+ at the same concentration. Therefore, spectral narrowing may be linked to loss of water-water hydrogen bonds, corresponding to negative interaction energies in Fig. S7 in *SI Appendix*, while shifting of the $3,400\ cm^{-1}$ peak may be loosely related to the less typical hydrogen bond interactions induced by ions. Dynamics and therefore changes of the vibrational lifetime may also account for some of the apparent spectral narrowing.

The change in water structure with increasing concentration of $MgCl_2$ is manifested in the radial distribution functions of water oxygen atoms around Mg^{2+} (*SI Appendix*). The first solvation shell of Mg^{2+} in the simulations contains six tightly-held water molecules, in agreement with previous simulations and experiment (7). The second solvation shell is well defined and similar at all of the concentrations considered. At 2.7 M $MgCl_2$ a shoulder appears just beyond the second solvation shell, indicating the emergence of additional long-range order. At 4.8 M additional peaks appear, signaling the dramatic restructuring (ordering) of water by high concentrations of $MgCl_2$. The number of waters coordinated by Cl^- diminishes near the Gibbs dividing surface from 7 to ~5 water molecules, and this reduction is only slightly concentration dependent (5.0–5.6 water at the interface).

Influence of Mg^{2+} on the Intensity of the Free OH Peak. The intensity of the free OH peak behaves differently than that of the hydrogen bonding region. There is a small decrease in SFG intensity with increasing concentration of $MgCl_2$ for concentrations up to 2.1 M. However, the number of free OH as seen in the MD simulations increases with concentration. This discrepancy has been previously attributed to red-shifting of free OH in the first solvation shell of Mg^{2+} out of the peak attributed to other free OH contributions, as well as to perturbations of the intensity of free OH stretches by ions (23, 24). For 3.1 M and 4.7 M $MgCl_2$, a larger decrease in SFG intensity of the free OH peak is observed relative to the lower concentrations. The free OH orientational distributions plotted in Fig. 4 show that, with increasing concentration, layers of free OH with opposing orientations appear. While there is a hint of stratification at 1.9 M, it is clearly evident in 2.7 M and 4.8 M $MgCl_2$. In fact, in the 4.8 M $MgCl_2$, there are no longer two regions of net orientation as seen in the lower concentrations, but four layers. The SFG signal from these layers of free OH with opposing orientation would be expected to interfere destructively, leading to a loss in SFG intensity in the free OH region in addition to that expected from frequency and intensity changes due to water-ion interactions.

Influence of Mg^{2+} on the Free OH Frequency. In the SFG spectra presented in Fig. 1*B*, we observe a peak at $3,650\ cm^{-1}$. To gain insight into the origin of this peak, ab initio calculations on Na^+ and Mg^{2+} with complete first solvation shells were performed (Table S5 in *SI Appendix*). Deuteration was used to decouple a single water or single OH oscillator in each cluster in an effort to mimic a free OH in solution, where other OH oscillators would be part of the hydrogen bonding network. The shift from the main free OH peak to the new peak at $3,650\ cm^{-1}$ seen in Fig. 1*B* is approximately $50\ cm^{-1}$. The difference in the OH stretch frequency in $Mg^{2+} \cdot HOD \cdot (D_2O)_5$ and $Na^+ \cdot HOD \cdot (D_2O)_5$ calculated at the MP2/aug-cc-pVDZ level of theory is $49\ cm^{-1}$. Hence, we conclude that water molecules in the first solvation shell of Mg^{2+} contribute to the $3,650\ cm^{-1}$ peak.

Aerosol Perspective. What have we learned about the surface of an atmospheric marine aerosol? The air/aqueous interface of a marine aerosol, based on our previous work (12, 13, 25), and the work presented here, is Cl^- and Mg^{2+} rich. Both ions will be further attracted toward the surface as the aerosol loses water during continental transport. Previously we have shown that in other solutions (12) the surface structure is highly influenced by the presence of the divalent magnesium cation, and that Cl^- does not form contact ion pairs with Mg^{2+} (7). Because Cl^- is closer to the interface in the presence of Mg^{2+}, as revealed here, the surface reactivity of MBL aerosol is likely enhanced when the aerosol passes over dryer continental regions as it is transported inland. However, in MBL aerosol with high fatty acid content, a fraction of the Mg^{2+} cations are trapped near the subsurface carboxylate and carboxylic acid groups of the fatty acids, where they could render these Mg^{2+} less potent with respect to their control over the positioning of Cl^-. In these cases, there is still a great deal that is not well understood with respect to aqueous surfaces. Water structure is highly perturbed, but it is not known if the Cl^- ions in these systems are more or less apt to exist in the very topmost layer of the surface. Krisch et al. recently showed that, while the strong enhancement of I^- at the air/aqueous interface was reduced by the surfactant butanol, a substantial population of I^- remained in the interfacial region (26). In previous work, we revealed that, even in highly packed fatty acid and lipid monolayers on aqueous surfaces, water molecules exist in the interstitial spaces, as evidenced by the observation of perturbed free OH (OD) bonds that interacted with the fatty acid tails (12, 27). Whether or not surfactant-like molecules act as a barrier to the uptake of atmospheric trace gases will depend on a number of factors such as surface density of the molecules, and the identity of the trace gas (28). The influence of surfactant-like molecules on the heterogeneous chemistry of ions in aqueous aerosols is a fruitful area for future research.

Materials and Methods

Materials. Magnesium chloride hexahydrate ($MgCl_2 \cdot 6H_2O$; ACS certified) was obtained from Fisher Scientific. Deuterated (D31) palmitic acid was obtained from Cambridge Isotopes. Deionized water was obtained from a Barnstead Nanopure filtration system with a minimum resistivity of 18.2 MΩ · cm. Details of solution preparation are found in *SI Appendix*.

Spectroscopy Methods. SFG spectra were acquired using a broad bandwidth SFG spectrometer described previously (12, 20, 29). All spectra were acquired at 22 ± 1 °C and in a range from 40 to 50% ambient relative humidity. Additional details can be found in *SI Appendix*.

Computational Methods. Interfacial simulations of aqueous $MgCl_2$, NaCl, and neat water employed a slab geometry with the unit cell dimensions 30 Å × 30 Å × 100 Å and three-dimensional periodic boundary conditions. The systems each contained 864 water molecules and 16, 33, 48, and 96 $MgCl_2$, corresponding to bulk concentrations of 1.1 M, 1.9 M, 2.7 M, and 4.8 M, respectively. The 4.9 M NaCl solution contained 864 water molecules and 96 NaCl. Details of the MD simulation protocols are provided in *SI Appendix*.

ACKNOWLEDGMENTS. The National Science Foundation (Grant CHE-0749807) and the Department of Energy (Grant DOE-BES DE-FB02-04ER15495) (to N.N.C.-I, C.Y.T, X.C., and H.C.A) supported this work. AirUCI (Atmospheric Integrated Research for Understanding Chemistry at Interfaces) helped to support this work with funding by the National Science Foundation (Grants CHE-0431312 and CHE-0909227)(to K.M.C., M.R., and D.J.T). K.M.C. is grateful for a fellowship from GAANN (Graduate Assistance in Area of National Need). Support from the Ministry of Education of the Czech Republic (Grants ME09064, LC512 and Z40550506) (to M.R.) is also gratefully acknowledged.

1. Blanchard D (1985) The oceanic production of atmospheric sea salt. *J Geophys Res* 90(C1):961–963.
2. Shaw G (1991) Aerosol chemical components in Alaska air masses 2. Sea salt and marine product. *J Geophys Res* 96(D12):22369–22372.
3. Foster P, et al. (2007) *Climate change 2007: The physical science basis. Intergovernmental panel on climate change* (Cambridge Univ Press, United Kindgdom and New York), pp 129–234.
4. Rosenfeld D, et al. (2008) Flood or drought: How do aerosols affect precipitation? *Science* 321(5894):1309–1313.
5. Kester DR, Duedall IW, Connors DN, Pytkowicz RM (1967) Preparation of artificial seawater. *Limnol Oceanogr* 12:176–179.
6. Lihavainen H, et al. (2008) Measurements of the relation between aerosol properties and microphysics and chemistry of low level liquid water clouds in Northern Finland. *Atmos Chem Phys* 8(23):6925–6938.
7. Callahan KM, Casillas-Ituarte NN, Roeselová M, Allen HC, Tobias DJ (2009) Solvation of magnesium dication: Molecular dynamics simulation and vibrational spectroscopic study of magnesium chloride in aqueous solutions. *J Phys Chem B*, in press.
8. Finlayson-Pitts BJ, Hemminger JC (2000) Physical chemistry of airborne sea salt particles and their components. *J Phys Chem A* 104(49):11463–11477.
9. Finlayson-Pitts BJ (1993) Chlorine atoms as a potential tropospheric oxidant in the marine boundary layer. *Res Chem Intermed* 19(3):235–249.
10. Wang J, Lee YN, Daum PH, Jayne J, Alexander ML (2008) Effects of aerosol organics on cloud condensation nucleus (CCN) concentration and first indirect aerosol effect. *Atmos Chem Phys* 8(21):6325–6339.
11. Tervahattu H, et al. (2002) New evidence of an organic layer on marine aerosols. *J Geophys Res* 107:AAC1–AAC9.
12. Allen HC, Casillas-Ituarte NN, Sierra-Hernández MR, Chen X, Tang CY (2009) Shedding light on water structure at air-aqueous interfaces: Ions, lipids, and hydration. *Phys Chem Chem Phys* 11(27):5538–5549.
13. Gopalakrishnan S, Liu D, Allen HC, Kuo M, Shultz MJ (2006) Vibrational spectroscopic studies of aqueous interfaces: Salts, acids, bases, and nanodrops. *Chem Rev* 106(4):1155–1175.
14. Sovago M, et al. (2008) Vibrational response of hydrogen-bonded interfacial water is dominated by intramolecular coupling. *Phys Rev Lett* 100(17):173901/1–173901/4.
15. Du Q, Superfine R, Freysz E, Shen YR (1993) Vibrational spectroscopy of water at the vapor/water interface. *Phys Rev Lett* 70(15):2313–2316.
16. Ji N, Ostroverkhov V, Tian CS, Shen YR (2008) Characterization of vibrational resonances of water-vapor interfaces by phase-sensitive sum-frequency spectroscopy. *Phys Rev Lett* 096102/1–096102/4.
17. Raymond EA, Richmond GL (2004) Probing the molecular structure and bonding of the surface of aqueous salt solutions. *J Phys Chem B* 108(16):5051–5059.
18. Bush MF, et al. (2009) Hydration of alkaline earth metal dications: Effects of metal ion size determined using infrared action spectroscopy. *J Am Chem Soc* 131:13270–13277.
19. Richmond GL (2002) Molecular bonding and interactions at aqueous surfaces as probed by vibrational sum frequency spectroscopy. *Chem Rev* 102(8):2693–2724.
20. Tang CY, Allen HC (2009) Ionic binding of K^+ and Na^+ to the carboxylic acid head group of palmitic acid in monolayers using vibrational sum frequency generation spectroscopy. *J Phys Chem A* 113(26):7383–7393.
21. Chaban GM, Jung JO, Gerber RB (2000) Anharmonic vibrational spectroscopy of hydrogen-bonded systems directly computed from ab initio potential surfaces: $(H_2O)_n$, $n = 2, 3$; $Cl^-(H_2O)_n$, $n = 1, 2$; $H^+(H_2O)_n$, $n = 1, 2$; H_2O-CH_3OH. *J Phys Chem A* 104:2772–2779.
22. Smith JD, Saykally RJ, Geissler PL (2007) The effects of dissolved halide anions on hydrogen bonding in liquid water. *J Am Chem Soc* 129:13847–13856.
23. Miller DJ, Lisy JM (2008) Hydrated alkali-metal cations: Infrared spectroscopy and ab initio calculations of $M^+(H_2O)_{x=2-5}Ar$ cluster ions for M = Li, Na, K, and Cs. *J Am Chem Soc* 130:15381–15392.
24. Probst MM, Hermansson K (1991) On frequency shifts in OH stretching vibrations of hydrated cations. *J Chem Phys* 96(12):8995–9004.
25. Mucha M, et al. (2005) Unified molecular picture of the surfaces of aqueous acid, base, and salt solutions. *J Phys Chem B* 109(16):7617–7623.
26. Krisch MJ, et al. (2007) The effect of an organic surfactant on the liquid-vapor interface of an electrolyte solution. *J Phys Chem C* 111:13497–13509.
27. Ma G, Chen X, Allen HC (2007) Dangling OD confined in a Langmuir monolayer. *J Am Chem Soc* 129:14053–14057.
28. Park S-C, Burden DK, Nathanson GM (2009) Surfactant control of gas transport and reactions at the surface of sulfuric acid. *Accounts Chem Res* 42:379–387.
29. Harper K, et al. (2009) Surface residence and uptake of methyl chloride and methyl alcohol at the air/water interface studied by vibrational sum frequency generation spectroscopy and molecular dynamics. *J Phys Chem A* 113(10):2015–2024.